Inorganic Chemistry

Article

pubs.acs.org/IC

Small Bifunctional Chelators That Do Not Disaggregate Amyloid β Fibrils Exhibit Reduced Cellular Toxicity

Anuj K. Sharma,[†] Jaekwang Kim,[‡] John T. Prior,[†] Nicholas J. Hawco,[†] Nigam P. Rath,[§] Jungsu Kim,[‡] and Liviu M. Mirica*,[†]

[†]Department of Chemistry, Washington University, One Brookings Drive, St. Louis, Missouri 63130-4899, United States

[‡]Department of Neurology, Washington University School of Medicine, St. Louis, Missouri 63108, United States

[§]Department of Chemistry and Biochemistry, University of Missouri—St. Louis, One University Boulevard, St. Louis, Missouri 63121-4400, United States

Supporting Information

ABSTRACT: Multifunctional metal chelators that can modulate the amyloid β (Aβ) peptide aggregation and its interaction with metal ions such as copper and zinc hold considerable promise as therapeutic agents for Alzheimer's disease (AD). However, specific rather than systemic metal chelation by these compounds is needed in order to limit any side effects. Reported herein are two novel small bifunctional chelators, 2-[2-hydroxy-4-(diethylamino)phenyl]benzothiazole (L1) and 2-(2-hydroxy-3-methoxyphenyl)benzothiazole (L2), in which the metal-binding donor atoms are integrated within a molecular framework derived from the amyloid-binding fluorescent dye thioflavin T (ThT). The metal-binding properties of L1 and L2 were probed by pH spectrophotometric titrations to determine their pK_a values and the corresponding metal complex stability constants, and the isolated metal complexes were structurally characterized. The amyloid-fibril-binding properties of L1 and L2 were investigated by fluorescence titrations and ThT competition assays. Interestingly, L1 and L2 do not lead to the formation of neurotoxic Aβ_{42} oligomers in the presence or absence of metal ions, as observed by native gel electrophoresis, Western blotting, and transmission electron microscopy. In addition, L1 and L2 were able to reduce the cell toxicity of preformed Aβ_{42} oligomers and of the copper-stabilized Aβ_{42} oligomers. Given their ability to reduce the toxicity of soluble Aβ_{42} and Cu-Aβ_{42} species, L1 and L2 are promising lead compounds for the development of chemical agents that can control the neurotoxicity of soluble Aβ_{42} species in AD.

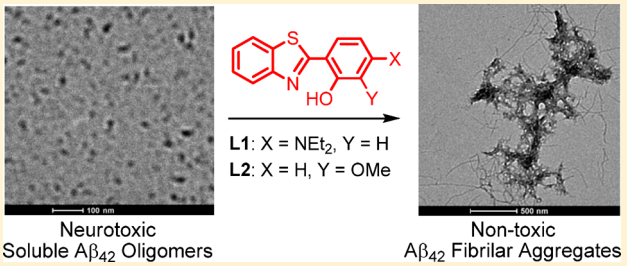

INTRODUCTION

More than 5 million people in the United States and 24 million worldwide are affected by Alzheimer's disease (AD), a disease characterized by memory loss and neurodegeneration.[1−3] Insoluble aggregates of the 42 and 40 amino acid long amyloid β peptides (Aβ_{42} and Aβ_{40}, respectively) are believed to be intimately involved in the onset of AD. However, while amyloid plaques, the ultimate product of Aβ aggregation, have been proposed to promote neurodegeneration and dementia,[4] recent studies have shown that the soluble Aβ oligomers are more neurotoxic both in vitro and in vivo.[5−8] In addition, while Aβ_{40} is present in larger amounts in amyloid plaques, the longer and more hydrophobic Aβ_{42} isoform has a higher tendency to generate neurotoxic oligomeric species.[9,10]

Interestingly, unusually high concentrations of copper, iron, and zinc have been found within the amyloid deposits in AD-affected brains.[11] These metal ions have been shown to affect Aβ aggregation, as well as lead to the formation of reactive oxygen species (ROS).[12−16] Although many studies have investigated the involvement of metal ions in Aβ aggregation and plaque formation, the molecular mechanisms of metal−Aβ species interactions, especially for the more neurotoxic Aβ_{42}, are still not completely understood. Exley et al. have used fluorescence assays and transmission electron microscopy (TEM) to show that both sub- and superstoichiometric concentrations of Cu^{2+} prevent aggregation of Aβ_{42} into thioflavin T (ThT)-positive β-sheet-rich amyloid fibrils.[17−19] We have also recently reported that Cu^{2+} ions slow down fibrillization of the Aβ_{42} peptide and stabilize the soluble Aβ_{42} species, as observed by native gel electrophoresis/Western blotting, TEM, cell viability studies,[20,21] and pulsed hydrogen/deuterium exchange mass spectrometry studies.[22] In this regard, metal chelators have been shown to reduce metal-mediated Aβ aggregation, ROS formation, and neurotoxicity in vitro.[23−26] Recent efforts to control abnormal Aβ−metal interactions have focused on small molecules, bifunctional chelators (BFCs), that have binding affinity for both metal ions and Aβ aggregates.[20,25,27−30] However, the majority of these BFCs have been studied for their effect on aggregation of the Aβ_{40} peptide,[25,31]

Received: April 21, 2014
Published: October 21, 2014

   dx.doi.org/10.1021/ic500926c | Inorg. Chem. 2014, 53, 11367−11376

and fewer studies have focused on their interaction with the more neurotoxic Aβ_{42} peptide.[20,21] Compounds that inhibit metal-mediated Aβ_{40} aggregation or promote disaggregation of amyloid fibrils were shown to lead to increased cell viability.[25,31,32] However, this approach may not be optimal for the Aβ_{42} peptide, given the increased toxicity observed for soluble Aβ_{42} oligomers.[20,21] Our current efforts are aimed at the development of BFCs that control the metal−Aβ_{42} neurotoxicity in vivo and take into consideration the formation of neurotoxic soluble Aβ_{42} oligomers and their proposed role in AD neuropathogenesis. Reported herein are two new BFCs, 2-[2-hydroxy-4-(diethylamino)phenyl]benzothiazole (L1) and 2-(2-hydroxy-3-methoxyhenyl)benzothiazole (L2), that were designed following a previously reported strategy of incorporating metal-binding atoms into the structural framework of an Aβ-interacting compound.[23,33,34] L1 and L2 have a modified 2-(2-hydroxyphenyl)benzothiazole (HPB) molecular framework reminiscent of the amyloid-binding fluorescent dye ThT (Scheme 1), which was shown to be promising in the design of new Aβ-binding compounds.[33] These BFCs fulfill the druglike criteria for further biological in vivo assays. The bifunctional character of the two compounds was confirmed by metal-chelating and Aβ-binding studies. The Cu^{2+} complexes of L1 and L2 were isolated and characterized spectroscopically and by X-ray structural determination. The amyloid-binding properties of L1 and L2 were explored by fluorescent titrations and by ThT competition assays. While L1 exhibits an acceptable binding affinity for Aβ fibrils, with the higher affinity binding site corresponding to a K_i of 260 nM, L2 binds very strongly to Aβ fibrils with a K_i of 15 nM. In addition, L1 and L2 moderately inhibit Aβ_{42} aggregation in the absence of metal ions, yet they promote aggregation in the presence of metal ions, as observed by native gel/Western blotting and TEM. In addition, L1 and L2 were able to reduce the cell toxicity of preformed Aβ_{42} oligomers as well as that of soluble copper-stabilized Aβ_{42} oligomers, which were shown recently to be neurotoxic.[20,21] These promising properties of L1 and L2 make them suitable candidates for further in vivo investigation.

Scheme 1. Molecular Structures of ThT, Pittsburgh Compound B (PiB), Clioquinol (CQ), and the BFCs L1 and L2 Described in This Work

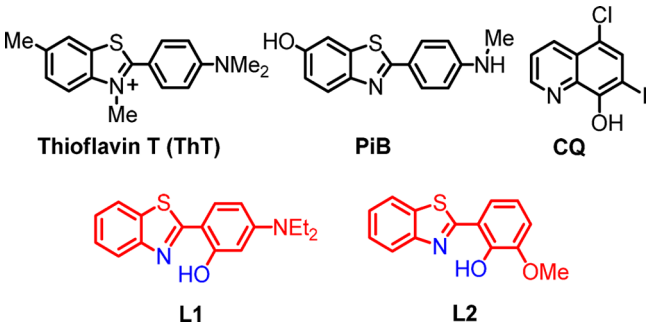

EXPERIMENTAL SECTION

General Methods. All reagents were purchased from commercial sources and used as received unless stated otherwise. Solvents were purified prior to use by passing through a column of activated alumina using an MBraun Solvent Purification System. All solutions and buffers were prepared using metal-free Millipore water that was treated with Chelex overnight and filtered through a 0.22 μm nylon filter. ^{1}H (300.121 MHz) and ^{13}C (75 MHz) NMR spectra were recorded on a Varian Mercury-300 spectrometer. Chemical shifts are reported in ppm and referenced to residual solvent resonance peaks. UV−vis spectra were recorded on a Varian Cary 50 Bio spectrophotometer and are reported as λ_{max}, nm (ε, M^{-1} cm^{-1}). Electrospray ionization mass spectrometry (ESI-MS) experiments were performed using a Bruker M-axis QTOF mass spectrometer with an ESI source. ESI-MS was provided by the Washington University Mass Spectrometry NIH Resource (Grant P41RR0954), and elemental analyses were carried out at Intertek Chemical and Pharmaceuticals testing and analysis services. TEM analysis was performed at the Nano Research Facility at Washington University.

X-ray Crystallography. Suitable crystals of appropriate dimensions were mounted in a Bruker Kappa Apex II CCD X-ray diffractometer equipped with an Oxford Cryostream LT device and a fine-focus Mo Kα radiation X-ray source (λ = 0.71073 Å). Preliminary unit cell constants were determined with a set of 36 narrow frame scans. Typical data sets consist of combinations of ϖ and ϕ scan frames with a typical scan width of 0.5° and a counting time of 15−30 s/frame at a crystal-to-detector distance of ~4.0 cm. The collected frames were integrated using an orientation matrix determined from the narrow frame scans. *Apex II* and *SAINT* software packages[35] were used for data collection and data integration. Final cell constants were determined by the global refinement of reflections from the complete data set. Data were corrected for systematic errors using *SADABS*.[35] Structure solutions and refinement were carried out using the *SHELXTL-PLUS* software package.[36] The structures were refined with full-matrix least-squares refinement by minimizing $\sum w(F_o^2 - F_c^2)^2$. All non-hydrogen atoms were refined anisotropically to convergence. All hydrogen atoms were added in the calculated position and refined using appropriate riding models (AFIX m^3). Additional crystallographic details can be found in the Supporting Information (SI).

Acidity and Stability Constant Determination. UV−vis pH titrations were employed for determination of the acidity constants of L1 and L2 and their stability constants with Cu^{2+} and Zn^{2+}. For the acidity constants, solutions of BFCs (25 μM for L1 and 50 μM for L2, 0.1 M NaCl, pH 3) were titrated with small aliquots of 0.1 M NaOH at room temperature. At least 30 UV−vis spectra were collected in the pH 3−11 range. Because of the limited solubility of L1 and L2 in water, methanol (MeOH) stock solutions (10 mM) were used and titrations were performed in a MeOH−water mixture in which MeOH did not exceed 20% (v/v). Similarly, the stability constants for the L1−copper system were determined by titrating a solution of L1 (25 μM) and $Cu(ClO_4)_2{\cdot}6H_2O$ (12.5 μM) with small aliquots of 0.1 M NaOH at room temperature. At least 30 UV−vis spectra were collected in the pH 3−11 range. The acidity and stability constants were calculated using the *HypSpec* computer program (Protonic Software GmbH, U.K.).[37] Speciation plots of the compounds and their metal complexes were calculated using the program *HySS2009* (Protonic Software GmbH, U.K.).[38]

Aβ Peptide Experiments. Aβ monomeric films were prepared by dissolving commercial Aβ_{42} (or Aβ_{40} for Aβ-fibril-binding studies) peptide (Keck Biotechnology Resource Laboratory, Yale University) in HFIP (1 mM) and incubating for 1 h at room temperature.[39] This solution was then aliquoted out, and HFIP was allowed to evaporate overnight. The aliquots were vacuum-centrifuged, and the resulting monomeric films were stored at −80 °C. Aβ fibrils were generated by dissolving monomeric Aβ films in dimethyl sulfoxide (DMSO), diluting into the appropriate buffer, and incubating for 24 h at 37 °C with continuous agitation (the final DMSO concentration was <2%). For metal-containing fibrils, the corresponding metal ions were added before initiation of the fibrillization conditions. For inhibition studies, BFCs (50 μM, DMSO stock solutions) were added to Aβ solutions (25 μM) in the absence or presence of metal salts ($CuCl_2$ or $ZnCl_2$, 25 μM) and incubated for 24 h at 37 °C with constant agitation. For disaggregation studies, the preformed Aβ fibrils in the absence or presence of metal ions were treated with BFCs and further incubated for 24 h at 37 °C with constant agitation. For the preparation of soluble Aβ_{42} oligomers, a literature protocol was followed.[7,39] A monomeric film of Aβ_{42} was dissolved in anhydrous DMSO, followed

dx.doi.org/10.1021/ic500926c | Inorg. Chem. 2014, 53, 11367−11376

by the addition of DMEM-F12 media [1:1 (v/v), without phenol red; Invitrogen]. The solution (50−100 μM) was incubated at 4 °C for 24 h and then centrifuged at 10000*g* for 10 min. The supernatant was used as a solution of soluble Aβ_{42} oligomers.

Fluorescence Measurements. All fluorescence measurements were performed using a SpectraMax M2e plate reader (Molecular Devices). For ThT fluorescence studies, samples were diluted to a final concentration of 2.5 μM Aβ in phosphate-buffered saline (PBS) containing 10 μM ThT and the fluorescence was measured at 485 nm (λ_{ex} = 435 nm). For Aβ-fibril-binding studies, a 5 μM Aβ fibril solution was titrated with small amounts of compound and their fluorescence intensity measured ($\lambda_{ex}/\lambda_{em}$ = 330/450 nm). For ThT competition assays, a 5 μM Aβ fibril solution with 2 μM ThT was titrated with small amounts of compound and the ThT fluorescence measured ($\lambda_{ex}/\lambda_{em}$ = 435/485 nm). For calculation of K_i values, a K_d value of 1.17 μM was used for the binding of ThT to Aβ_{40} fibrils.[20,21]

TEM. Glow-discharged grids (Formar/Carbon 300 mesh, Electron Microscopy Sciences) were treated with Aβ samples (25 μM, 5 μL) for 2−3 min at room temperature. Excess solution was removed using filter paper, and grids were rinsed twice with water (5 μL). Grids were stained with uranyl acetate (1% w/v, water, 5 μL) for 1 min, blotted with filter paper, and dried for 15 min at room temperature. Images were captured using a FEI G2 Spirit Twin microscope (60−80 kV, 6500−97000× magnification).

Native Gel Electrophoresis and Western Blotting. All gels, buffers, membranes, and other reagents were purchased from Invitrogen and used as directed except where otherwise noted. Samples were separated on 10−20% gradient Tris-tricine minigels. The gel was transferred to a nitrocellulose membrane in an ice bath, and the protocol was followed as suggested except that the membrane was blocked overnight at 4 °C. After blocking, the membrane was incubated in a solution (1:2000 dilutions) of 6E10 anti-Aβ primary antibody (Covance) for 3 h. Invitrogen's Western Breeze Chemiluminescent kit was used to visualize the bands. An alkaline/phosphatase antimouse secondary antibody was used, and the protein bands were imaged using a Fujifilm LAS-1000CH luminescent image analyzer.

Cytotoxicity Studies (Alamar Blue Assay). Mouse neuroblastoma Neuro2A (N2A) cell lines were purchased from the American Type Culture Collection (ATCC). Cells were grown in DMEM/10% FBS, which is the regular growth media for N2A cells. N2A cells were plated to each well of a 96-well plate (2.5×10^4/well) with DMEM/10% FBS. The media was changed to DMEM/N2 media 24 h later. After 1 h, the reagents (20 μM Aβ_{42} species, compounds, and metals) were added. Because of the poor solubility of the compounds in water or media, the final amount of DMSO used was 1% (v/v). After an additional incubation of 40 h, the Alamar Blue solution was added in each well and the cells were incubated for 90 min at 37 °C. The absorbance was measured at 570 nm (control optical density = 600 nm). For these toxicity studies, three types of Aβ_{42} species were tested: freshly made monomeric Aβ_{42} (MAβ_{42}), Aβ_{42} oligomers (OAβ_{42}), and Aβ_{42} fibrils (FAβ_{42}). These Aβ_{42} species were prepared as described above.

Synthesis of L1. A mixture of 2-aminothiophenol (2.5 g, 20 mmol) and (diethylamino)salicylaldehyde (3.86 g, 20 mmol) in DMSO (20 mL) was heated with stirring at 150 °C for 6 h under dinitrogen. Then it was cooled to 0 °C for 8 h, and the orange solid crystallized out, was collected by filtration, and was washed with hexane (2.97 g, yield 50%). ^{1}H NMR ($CDCl_3$): δ 7.85 (d, 1H, ArH), 7.81 (d, 1H, ArH), 7.46 (d, 1H, ArH), 7.43 (d, 1H, ArH), 7.30 (d, 1H, phenol H), 6.30 (d, 1H, phenol H), 6.27 (s, 1H, phenol H), 3.41 (q, 2H, CH_2CH_3), 1.22 (t, 3H, CH_2CH_3). ^{13}C NMR ($CDCl_3$): δ 169.78, 159.98, 152.43, 151.52, 132.08, 130.04, 126.42, 124.35, 121.40, 121.18, 105.96, 104.34, 98.053, 44.72, 12.86. UV−vis [λ_{max}, nm, (ε, M^{-1} cm^{-1})]: in MeCN, 262 (10300), 380 (43000); in PBS, 272 (9500), 375 (18000), 405 (19500). HRMS. Calcd for $[M + H]^+$: m/z 299.1218. Found: m/z 299.1225.

Synthesis of L2. A mixture of *o*-vanilin (2.0 g, 0.0131 mol) and 2-aminothiophenol (1.64 g, 0.0131 mol) in ethanol (15 mL) was refluxed with stirring for 24 h. Then it was cooled to room temperature and poured in water. The sticky yellow solid was crystallized from MeOH to obtain yellow crystals (1.15 g, yield 37%). ^{1}H NMR ($CDCl_3$): δ 8.02 (d, 1H, ArH), 7.91 (d, 1H, ArH), 7.52 (t, 1H, ArH), 7.42 (t, 1H, ArH), 7.33 (d, 1H, ArH), 7.01 (d, 1H, ArH), 6.99 (t, 1H, ArH), 3.97 (s, 3H, OCH_3). ^{13}C NMR ($CDCl_3$): δ 169.28, 151.50, 148.93, 148.19, 148.17, 132.59, 126.70, 125.56, 122.16, 121.45, 119.98, 119.14, 116.71, 114.06, 56.22. UV−vis [λ_{max}, nm, (ε, M^{-1} cm^{-1})]: in MeCN, 307 (br, 10200), 340 (sh, 5500); in PBS, 305 (3500), 340 (sh, 1800), 390 (800). HRMS. Calcd for $[M + H]^+$: m/z 258.0588. Found: m/z 258.0584.

*Synthesis of [(L1)$_2$Cu^{II}]·0.5H$_2$O (**1**).* A solution of $CuCl_2 \cdot 2H_2O$ (0.011 g, 0.084 mmol) in MeCN (2 mL) was added to the stirring mixture of L1 (0.050 g, 0.167 mmol) and Et_3N (0.036 g, 0.334 mmol) in MeCN (5 mL). The brown precipitate immediately obtained was filtered, washed with ether, and dried under vacuum (0.040 g, yield 54%). UV−vis [λ_{max}, nm, (ε, $M^{-1}cm^{-1}$)]: in MeCN, 273 (sh, 18000), 391 (56800), 404 (sh, 50500), 540 (900). HRMS. Calcd for $[M + H]^+$: m/z 658.1497. Found: m/z 658.1492. Anal. Calcd for $C_{34}H_{34}N_4O_2S_2Cu \cdot 0.5H_2O$: C, 61.52; H, 5.25; N, 8.44. Found: C, 61.63; H, 6.11; N, 8.44.

*Synthesis of [(L1)Zn^{II}(Cl$_2$)](Et$_3$NH) (**2**).* A solution of $ZnCl_2$ (0.011 g, 0.084 mmol) in MeCN (2 mL) was added to the stirring mixture of L4 (0.050 g, 0.167 mmol) and Et_3N (0.018 g, 0.167 mmol) in MeCN (5 mL). The red solution was kept for slow evaporation, and a few single crystals were obtained within 2 days (0.052 g, yield 58%). UV−vis [λ_{max}, nm, (ε, $M^{-1}cm^{-1}$)]: in MeCN, 265 (19900), 391 (51000). ESI-MS. Calcd for [(L1)ZnCl + H]$^+$: m/z 397.01. Found: m/z 397.01. Satisfactory elemental analysis data could not be obtained because of the presence of a small amount of free ligand.

*Synthesis of [(L2)$_2$Cu^{II}]·0.5H$_2$O (**3**).* A solution of $CuCl_2 \cdot 2H_2O$ (0.013 g, 0.097 mmol) in MeCN (2 mL) was added to the stirring mixture of L2 (0.050 g, 0.194 mmol) and Et_3N (0.078 g, 0.776 mmol) in MeOH (10 mL). The brown precipitate immediately obtained was filtered, washed with ether, and dried under vacuum (0.051 g, yield 91%). UV−vis [λ_{max}, nm, (ε, $M^{-1}cm^{-1}$)]: in MeCN, 398 (26200), 515 (sh, 800), 700 (350). ESI-MS. Calcd for $[M + Na]^+$: m/z 598.0. Found: m/z 598.1. Anal. Calcd for $C_{28}H_{20}N_2O_4S_2Cu \cdot 0.5H_2O$: C, 57.47; H, 3.62; N, 4.79. Found: C, 57.34; H, 3.62; N, 4.83.

RESULTS AND DISCUSSION

Design, Synthesis, and Characterization of L1 and L2. Herein we employed the strategy of developing metal BFCs with amyloid-binding properties as potential therapeutic agents for AD. The fluorescent dye ThT is well-known for its amyloid-binding properties because of the 2-phenylbenzothiazole aromatic framework. Previously, an iodinated HPB and a few related compounds were shown to have potential as metal-chelating agents by Rodríguez-Rodríguez et al.[33] However, in that report, only the solution coordination properties of those compounds were investigated in detail, while the Aβ-binding and antiaggregation properties were only qualitatively evaluated through epifluorecense microscopy and turbidity assays. In contrast, in addition to the solution coordination chemistry, we have also determined the solid-state structure of the copper and zinc complexes of our compounds, and we have also quantitatively determined their Aβ-binding affinities through fluorescence titrations. In addition, we have used both TEM and gel electrophoresis/Western blotting to provide a complete picture of the effect of our compounds on Aβ aggregation and formation of various sized Aβ aggregates, in both the absence and presence of metal ions. Most importantly, we have correlated the in vitro studies with cellular toxicity studies, thus making this work a comprehensive study of these compounds in the context of developing new compounds that can control the toxicity and aggregation of various Aβ species. We have also recently reported 2-phenylbenzothiazole/

dx.doi.org/10.1021/ic500926c | Inorg. Chem. 2014, 53, 11367−11376

vanillin derivatives as BFCs that showed a strong affinity for Aβ fibrils.[20] Herein we designed two new molecules, L1 and L2, that contain a 2-phenylbenzothiazole moiety for Aβ recognition and oxygen- and nitrogen-atom donors needed for metal chelation. Synthesis of L1 and L2 was accomplished upon oxidative cyclization of the corresponding arylaldehyde and 2-aminothiophenol (Scheme S1 in the SI).[40] These compounds exhibit UV absorption in MeCN at 260 and 380 nm for L1 and at 305 and 345 nm for L2 (Figures S1 and S2 in the SI).[40] While both L1 and L2 are 2-phenylbenzothiazole derivatives, L1 exhibits low-intensity emission at 450 nm and a shoulder at 525 nm, yet L2 shows a more intense emission at 525 nm in PBS (Figures S3 and S4 in the SI).[40] The parent molecule HPB has emission properties similar to those of L2 (Figure S4 in the SI), which suggests that having a diethylamino group in L1 strongly affects its emission properties.

Another important aspect of the design of new drug molecules for central nervous system diseases is their ability to cross the blood brain barrier (BBB).[13,26,41] Both L1 and L2 are small in size, and they also satisfy Lipinski's rules for crossing the BBB (Table 1). The ability of a compound to cross

Table 1. Lipinski Parameters for L1 and L2

property	L1	L2	Lipinski's rule[a]
MW	298.41	257.31	≤500
c log *P*	4.853	3.834	≤5
HBD	1	1	≤5
HBA	3	3	≤10
PSA	36.36	42.35	≤70 Å^2
log BB	0.330	0.087	>−0.3

[a]MW = molecular weight; *c* log *P* = calculated octanol−water partition coefficient; HBD = hydrogen-bonding donor atoms; HBA = hydrogen-bonding acceptor atoms; PSA = polar surface area; log BB = −0.0148PSA + 0.152 *c* log *P* + 0.130 (Lipinski, C. A.; Lombardo, F.; Dominy, B. W.; Feeney, P. J. *Adv. Drug Delivery Rev.* **1997**, 23, 3−25; Clark, D. E.; Pickett, S. D. *Drug Discovery Today* **2000**, 5, 49−58).

the BBB can be evaluated by determining the blood−brain partitioning parameter log BB that is determined by taking into account the molecular weight of the molecule, charge, lipophilicity, and its hydrogen-bonding capability. Molecules having log BB values higher than −0.3 are generally expected to cross the BBB.[33] The calculated log BB values for L1 and L2 are +0.33 and +0.087, respectively, suggesting that these BFCs are expected to cross the BBB.

Acidity Constants of L1 and L2. Because both L1 and L2 contain functional groups that can undergo protonation, the acidity constants (pK_a) were determined by UV−vis spectrophotometric titrations. For both L1 and L2, UV−vis titrations from pH 3.0 to 11.0 reveal several changes in the spectra (Figures 1 and 2). For L1, the best fit to the data was obtained with pK_a values of 3.556(2), 8.427(3), and 10.108(2) (Table 2). The first and second pK_a values can be assigned to deprotonation of the nitrogen atoms of the benzothiazole and diethylamino groups, while the largest pK_a value is likely due to phenol deprotonation.[25,42] For L2, the best fit to the data was obtained with two pK_a values of 3.154(2) and 9.360(1) (Table 2). These pK_a values can be assigned to deprotonation of the nitrogen atoms of the benzothiazole and phenol groups, respectively.

Characterization of Metal Complexes. The BFCs L1 and L2 were explored for their ability to chelate metal ions. The

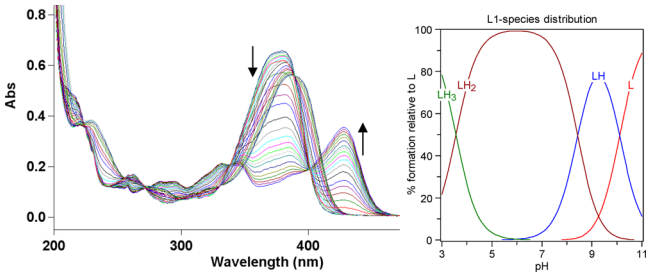

Figure 1. Variable-pH UV spectra of L1 (25 μM, 25 °C, I = 0.1 M NaCl) and the species distribution plot.

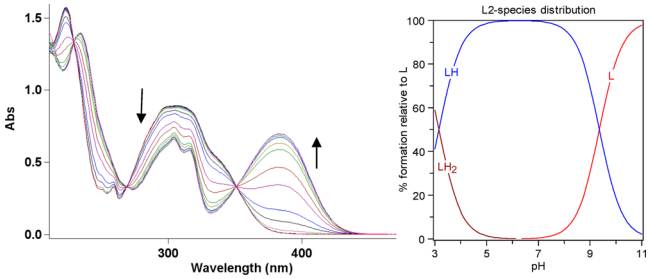

Figure 2. Variable-pH UV spectra of L2 (50 μM, 25 °C, I = 0.1 M NaCl) and the species distribution plot.

Table 2. Acidity Constants (pK_a Values) of L1 and L2 Determined by Spectrophotometric Titrations (Errors Are for the Last Digit)[a]

reaction	L1	L2
$[H_3L]^{2+} = [H_2L]^+ + H^+$ (pK_{a1})	3.556(2)	
$[H_2L]^+ = [HL] + H^+$ (pK_{a2})	8.427(3)	3.154(2)
$[HL] = [L]^- + H^+$ (pK_{a3})	10.108(2)	9.360(1)

[a][HL] represents the neutral form of L1 and L2.

stoichiometry of L1−Cu^{2+} and L1−Zn^{2+} complexes in solution was determined by Job's plot analysis.[43] For L1−Cu^{2+}, a break in the plot at 0.4 mole fraction of Cu^{2+} suggests the formation of both 1:1 and 2:1 L1−Cu^{2+} complexes in solution (Figure S4 in the SI).[40] For L1−Zn^{2+}, the break occurs at ∼0.3 mole fraction of Zn^{2+}, suggesting the formation of a 2:1 L1−Zn^{2+} complex (Figure S5 in the SI).[40] By contrast to L1, no Job's plot analysis could be performed for L2−Cu^{2+} because of the limited solubility of this complex, while no significant spectral change was observed for the L2−Zn^{2+} system. The Cu^{2+} complexes of L1 or L2 were synthesized by reacting $CuCl_2 \cdot 2H_2O$ with the corresponding ligand in MeCN in the presence of an equivalent amount of Et_3N. The 2:1 complex formation was confirmed by the ESI-MS signal at m/z 658.1 corresponding to $[M + H]^+$, which was further supported by X-ray structural determination (see below). The UV−vis spectrum of the L1−Cu^{2+} complex **1** reveals a d−d transition at ∼700 nm and a more intense band at 540 nm, while a phenolate-to-Cu^{2+} charge-transfer band is observed at ∼400 nm (Figure S6 in the SI).[40] Similarly, the UV−vis spectrum of the L2−Cu^{2+} complex **3** shows characteristic d−d transition bands at 700 and 515 nm as well as a phenolate-to-Cu charge-transfer band at ∼400 nm (Figure S7 in the SI).[40] Although a single crystal suitable for X-ray crystallography could be obtained from the reaction mixture of L1 and Zn^{2+}, the isolation of the zinc complexes of L1 or L2 did not lead to pure complexes to allow for their complete characterization.

dx.doi.org/10.1021/ic500926c | *Inorg. Chem.* 2014, 53, 11367−11376

Spectrophotometric titrations were also performed to determine the stability constants and solution speciation of Cu^{2+} with L1. The pK_a values of the ligands were included in the calculations,[42] and the best fit to the data shows that L1 binds Cu^{2+} with a stability constant of 11.99(2) for the M + L = ML equilibrium and a value of 20.99(2) for the ML + L = ML_2 equilibrium (L represents the deprotonated form of L1). The speciation diagram for the Cu−L1 system is shown in Figure 3.

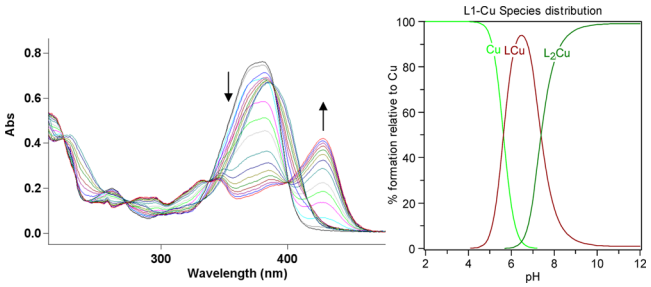

Figure 3. Variable-pH UV spectra of the L1−Cu^{2+} system ([L1] = 25 μM; [Cu^{2+}] = 12.5 μM, 25 °C, I = 0.1 M NaCl) and the species distribution plot.

In addition, the concentration of free Cu^{2+} (pCu = −log [Cu_{free}]) can be determined at specific pH values and total ion concentrations, with pCu values of 6.7 and 8.2 being determined for the Cu−L1 system at pH 6.6 and 7.4, respectively. These pCu values are lower compared to those for the analogous HPB compound reported previously,[33] likely because of the strong electron-withdrawing effect of the diethylamine group upon protonation. Unfortunately, the spectrophotometric titration of L2 in the presence of Cu^{2+} revealed few spectral changes at micromolar concentrations, while the use of higher concentrations led to precipitation of the L2−Cu^{2+} complex. However, it is expected that L2 exhibits a higher binding affinity to Cu^{2+} than L1 because of the electron-donating *o*-methoxy group present in L2. In addition, almost no changes were observed in the spectra of both L1 and L2 upon the addition of Zn^{2+}; therefore, the corresponding stability constants could not be determined. Attempts were then made to determine the apparent stability constants for the Zn−L1 and Zn−L2 complexes by using competition assays with a zinc chelator, zincon. Zincon was used previously by Faller et al. in Zn−Aβ interaction studies and exhibits a $K_d \approx 10$ μM for zinc.[44] In our case, the addition of zincon to solutions of Zn−L1 and Zn−L2 complexes results in quantitative formation of the Zn−zincon complex. In addition, L1 and L2 do not compete significantly with zincon for zinc binding, even when present in large excess versus zincon, suggesting that they exhibit affinities for zinc that are at least 10 times lower than that of zincon.

X-ray Structure of Metal Complexes. To further characterize the metal-binding properties of compounds L1 and L2, single-crystal X-ray structures were determined for complexes **1**−**3** (Figure 4 and Tables S1−S3 in the SI).[40] Complex **1** affords single crystals by Et_2O diffusion into a CH_2Cl_2 solution of **1** that crystallized out in the $C2/c$ space group. An oxygen atom and a nitrogen atom from two ligand molecules coordinate to Cu^{2+}. The Cu−O1 and Cu−N1 bond lengths are 1.980(3) and 1.876(2) Å, respectively, and the trans angles O1−Cu1−O1#1 and N1#1−Cu1−N1 are 153.3(2)° and 154.2(2)°, respectively, with these parameters suggesting a distorted square-planar geometry for Cu^{2+}. For complex **2**, the

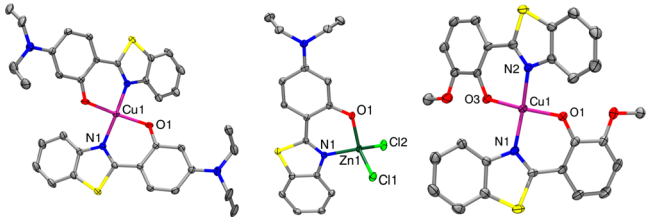

Figure 4. ORTEP representations (50% probability ellipsoids) of complexes **1**−**3**. All hydrogen atoms, counterions, and solvent molecules are omitted for clarity. Selected bond distances: **1**, Cu1−N1 1.980(3), Cu1−O1 1.876(2); **2**, Zn−N1 2.005(1), Zn−O1 1.956(1), Zn−Cl(1) 2.233(1), Zn−Cl(2) 2.222(1); **3**, Cu1−N1/N2 1.965(4), Cu1−O1/O3 1.873(4).

Zn^{2+} ion exhibits a distorted tetrahedral geometry and is coordinated to the benzothiazole nitrogen and phenol oxygen atoms of L1 and two chloride ions. The copper complex **3** afforded single crystals by Et_2O diffusion into a CH_2Cl_2 solution and has structural properties similar to those of **1**, yet it crystallized out in the $P2/n$ space group. As shown for **1**, in **3** an oxygen atom and a nitrogen atom from two ligand molecules coordinate to Cu^{2+}. The Cu−O1 and Cu−N1 bond lengths are 1.873(4) and 1.965(4) Å, respectively, and the trans angles O1−Cu1−O1#1 and N1#1−Cu1−N1 are 145.1(2)° and 146.2(2)°, respectively, reflecting a distorted square-planar geometry for Cu^{2+}.

Interaction of L1 and L2 with Aβ Species. Both compounds L1 and L2 contain a 2-phenylbenzothiazole fragment reminiscent of the fluorescent dye ThT used to detect the β-sheet structure of fibrillar Aβ aggregates.[45,46] In this context, the affinity of L1 and L2 toward Aβ fibrils was investigated by fluorescence assays. These studies were performed with $A\beta_{40}$ fibrils, which form more homogeneous fibrillar structures without any nonfibrillar aggregates.[45,47] Titration of L1 with Aβ fibrils was performed, and a saturation behavior is observed. The data were fitted with a one-site binding model to give a K_d of 4.70 ± 0.30 μM (Figure 5a), which suggests a moderate affinity of L1 for the Aβ fibrils. ThT fluorescence competition assays were also performed by the addition of L1 to a solution of Aβ fibrils in the presence of ThT. L1 shows a decrease in ThT fluorescence upon the addition of nanomolar amounts. Competitive-binding curve fitting yields a K_i value of 260 ± 40 nM (Figure 5b). It should be noted that the K_i value for L1 is smaller than the K_d value, which is most likely due to the fact that ThT binds with different affinities to more than one site to the Aβ fibrils.[47] As such, we propose that L1 replaces ThT only from the higher affinity binding site. By constrast, L2 did not show any significant increase in the fluorescence intensity in the presence of Aβ fibrils yet replaces ThT from the Aβ fibrils and exhibits a K_i value of 15 ± 10 nM, indicating a very strong binding affinity to Aβ fibrils (Figure 5c).

Effect of L1 and L2 on Aβ_{42} Aggregation. To investigate the effect of L1 and L2 on Aβ aggregation, we performed both inhibition and disaggregation studies (Scheme 3). Importantly, the $A\beta_{42}$ peptide was employed in these studies because it was shown to form neurotoxic soluble Aβ oligomers.[5,8,48] For inhibition experiments, freshly prepared $A\beta_{42}$ fibrils were treated with metal ions, BFCs, or both, and the reactions was monitored by ThT fluorescence, native gel electrophoresis/Western blotting analysis, and TEM.

dx.doi.org/10.1021/ic500926c | Inorg. Chem. 2014, 53, 11367−11376

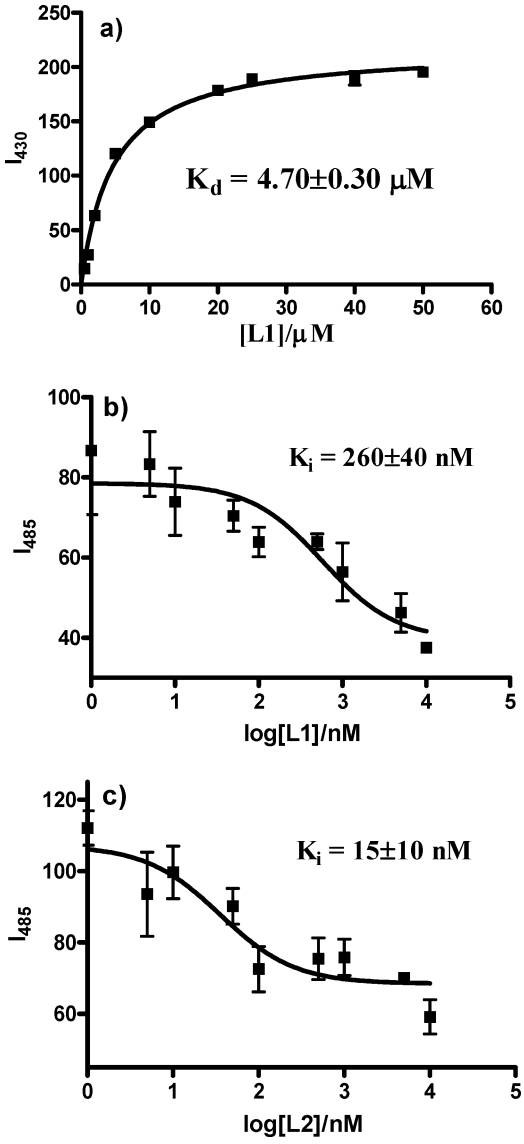

Figure 5. (a) Fluorescence titration assay of L1 with Aβ fibrils ([Aβ] = 5 μM; $\lambda_{ex}/\lambda_{em}$ = 330/450 nm). ThT fluorescence competition assays of Aβ fibrils with (b) L1 and (c) L2 ([Aβ] = 2 μM; [ThT] = 1 μM; $\lambda_{ex}/\lambda_{em}$ = 435/485 nm).

Scheme 3. Schematic Description of the Performed Inhibition and Disaggregation Experiments

Inhibition:

$A\beta_{42} + M^{2+} \xrightarrow[24\ h,\ 37\ °C\ agitation]{L1\ or\ L2} A\beta_{42}$ species

Disaggregation:

$A\beta_{42} + M^{2+} \xrightarrow[24\ h,\ 37\ °C\ agitation]{} A\beta_{42}$ aggregates $\xrightarrow[24\ h,\ 37\ °C\ agitation]{L1\ or\ L2} A\beta_{42}$ species

In inhibition experiments, a reduced ThT fluorescence was observed for the Cu^{2+}- and Zn^{2+}-containing fibrils, as reported previously (Figure 6).[21,49,50] In the absence of metal ions, the presence of L1 leads to a low ThT fluorescence intensity, while L2 has a negligible effect on Aβ_{42} fibrillization, suggesting that L1 can inhibit fibrillization more efficiently than L2. In the presence of Cu^{2+} and either L1 or L2, a very low ThT fluorescence intensity is observed, which could be due to either

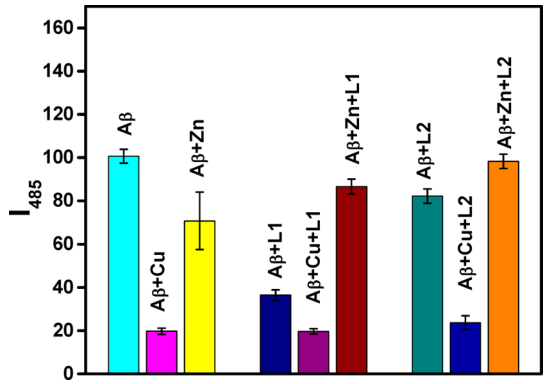

Figure 6. Normalized ThT fluorescence of the inhibition of Aβ fibrillization, measured upon incubaton at 37 °C for 24 h. Samples are as indicated on top of the lanes (PBS; [Aβ] = 25 μM; [M^{2+}] = 25 μM; [compound] = 50 μM).

limited Aβ_{42} fibril formation or fluorescence quenching by the paramagnetic Cu^{2+} ions. By comparison, the presence of Zn^{2+} and either L1 or L2 shows almost no effect on the ThT fluorescence intensity (Figure 6). Because the ThT fluorescence assays do not show a complete picture of the effect of BFCs on Aβ_{42} aggregation, native gel electrophoresis/Western blotting analysis and TEM were employed in order to characterize in more detail the various Aβ_{42} species formed during these aggregation studies. As such, the Aβ_{42} peptide forms well-defined Aβ_{42} fibrils, as confirmed by TEM (Figure 7, panel 1), while Aβ_{42} aggregation in the presence of Cu^{2+} shows the formation of a dramatically reduced number of Aβ_{42} fibrils (Figure 7, panel 2), thus supporting the low ThT fluorescence intensity observed above. By comparison, aggregation of Aβ_{42} in the presence of Zn^{2+} leads to the formation of large amorphous aggregates (Figure 7, panel 3). Native gel/Western blotting analysis shows that aggregation of Aβ_{42} in the absence of metal ions also forms high-molecular-weight oligomers, along with the insoluble aggregates that are observed at the top of the blot because they do not enter the gel (Figure 7, lane 1). As reported previously,[20,21] the presence of Cu^{2+} ions inhibits the formation of large soluble and insoluble Aβ_{42} aggregates (Figure 7, lane 2).

The presence of either L1 or L2 in the absence of metal ions does not seem to significantly inhibit Aβ_{42} aggregation, although some morphological changes were observed for the Aβ_{42} fibrils (Figure 7, panels 4 and 7); the observed decrease in the ThT fluorescence intensity may thus be due to these morphological changes of the Aβ_{42} aggregates. Native gel/Western blotting analysis reveals a limited effect of L1 and L2 on Aβ_{42} aggregation (Figure 7, lanes 4 and 7). Interestingly, the presence of either L1 or L2 has a dramatic effect on the Cu^{2+}-mediated oligomerization of Aβ_{42} and promotes the formation of larger Aβ_{42} aggregates, as observed by TEM (Figure 7, panels 5 and 8). Importantly, native gel/Western blotting analysis reveals bands at the top of the gel, suggesting the presence of insoluble Aβ_{42} aggregates (Figure 7, lanes 5 and 8), which were not observed in the presence of Cu^{2+} alone (Figure 7, lane 2). Thus, compounds L1 and L2 reduce the amount of soluble Aβ_{42} oligomers formed in the presence of Cu^{2+} by promoting the formation of insoluble Aβ_{42} aggregates. In addition, the presence of either L1 or L2 does not dramatically affect the formation of insoluble Aβ_{42} aggregates in the presence of Zn^{2+} (Figure 7, panels 6 and 9), which is supported by native gel/

dx.doi.org/10.1021/ic500926c | Inorg. Chem. 2014, 53, 11367−11376

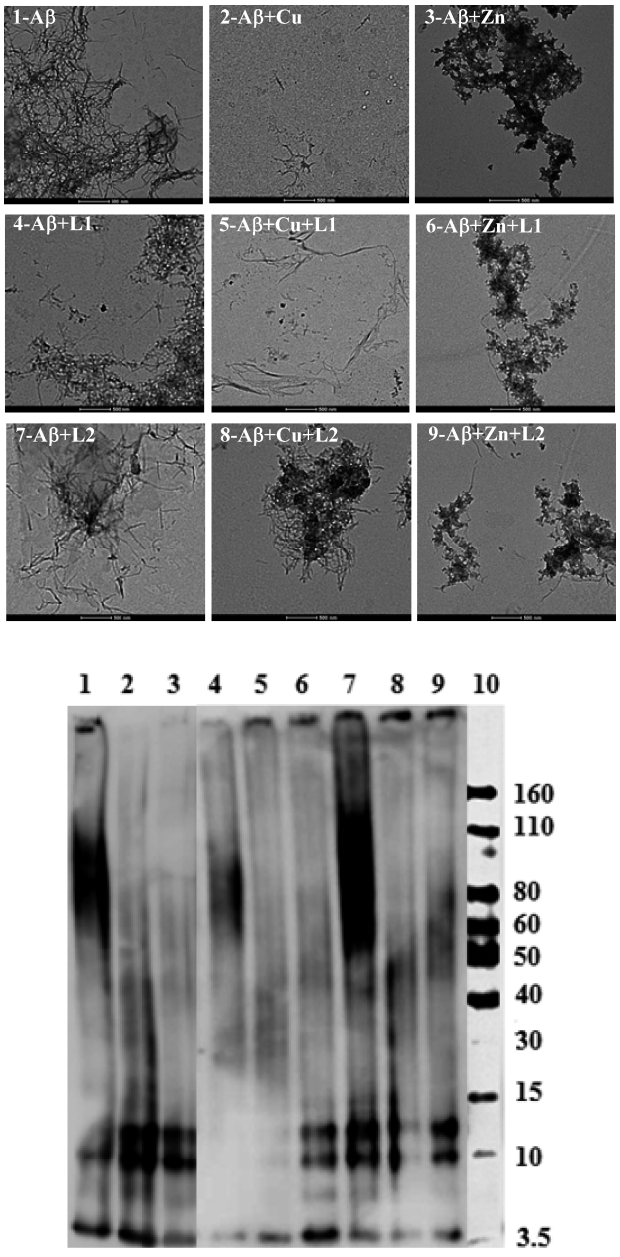

Figure 7. Top: TEM images of the inhibition of $A\beta_{42}$ aggregation by L1 and L2, in the presence or absence of metal ions ($[A\beta_{42}] = [M^{2+}] = 25\ \mu M$; [compound] = 50 μM; PBS, 37 °C, 24 h, scale bar = 500 nm). Bottom: Native gel electrophoresis/Western blotting analysis. Panels and lanes are as follows: (1) $A\beta_{42}$; (2) $A\beta_{42} + Cu^{2+}$; (3) $A\beta_{42} + Zn^{2+}$; (4) $A\beta_{42}$ + L1; (5) $A\beta_{42}$ + L1 + Cu^{2+}; (6) $A\beta_{42}$ + L1 + Zn^{2+}; (7) $A\beta_{42}$ + L2; (8) $A\beta_{42}$ + L2 + Cu^{2+}; (9) $A\beta_{42}$ + L2 + Zn^{2+}; (10) MW marker.

Western blotting analysis showing no formation of high-molecular-weight soluble $A\beta_{42}$ oligomers, although insoluble aggregates are observed at the top of the gel (Figure 7, lanes 6 and 9). Overall, these studies suggest that the presence of either L1 or L2, in both the presence or absence of metal ions, does not promote the formation of soluble $A\beta_{42}$ oligomers. Because the soluble $A\beta_{42}$ oligomers are the most neurotoxic species, these compounds are expected to control the neurotoxicity of $A\beta_{42}$ species in the presence of metal ions (vide infra).

Effect of L1 and L2 on $A\beta_{40}$ Aggregation. Although it was shown in previous studies[9,10,21] that the $A\beta_{42}$ peptide is more prone to form neurotoxic soluble $A\beta$ oligomers than the $A\beta_{40}$ peptide, we have also investigated the effect of L1 and L2 on the metal-mediated aggregation of $A\beta_{40}$. TEM analysis shows that $A\beta_{40}$ forms well-defined fibrils either in the absence or presence of L1 or L2 (Figure S9 in the SI, panels 1 and 4). Importantly, the presence of Cu^{2+} and Zn^{2+} does not inhibit $A\beta_{40}$ aggregation,[21] yet they change the morphology of the insoluble aggregates that become more amorphous (Figure S9 in the SI, panels 2 and 3). Moreover, in the presence of Cu^{2+} and either L1 or L2, a small amount of $A\beta_{40}$ fibrils are still formed (Figure S9 in the SI, panels 5 and 8), while the presence of Zn^{2+} and either L1 or L2 leads to the formation of a larger amount of fibrillar or amorphous aggregates, respectively (Figure S9 in the SI, panels 6 and 9). The TEM results are also supported by native gel electrophoresis/Western blotting analysis (Figure S10 in the SI), although this is less informative than in the case of the $A\beta_{42}$ peptide because of the lack of formation of an appreciable amount of soluble $A\beta$ oligomers under any experimental conditions. Therefore, because we are particularly interested in evaluating the role of metal ions and bifunctional compounds in controlling the formation of the neurotoxic soluble $A\beta$ oligomers, the $A\beta_{42}$ peptide was employed in the additional studies described below.

Disaggregation of $A\beta_{42}$ Fibrils. The effect of L1 and L2 on preformed $A\beta_{42}$ fibrils was also investigated in both the absence and presence of metal ions (Scheme 3). For disaggregation studies, $A\beta_{42}$ fibrils were prepared by incubation for 24 h at 37 °C, in both the presence and absence of metal ions. Then, L1 or L2 was added and further incubated for an additional 24 h at 37 °C. TEM and native gel electrophoresis/Western blotting characterization was performed on all of these samples. First, either L1 or L2 in metal-free conditions does not disaggregate the preformed $A\beta_{42}$ fibrils to an appreciable extent. Only some morphological changes were observed even after 24 h of incubation, and a significant amount of $A\beta_{42}$ aggregates were still observed by TEM (Figure 8, panels 4 and 7). Native gel electrophoresis/Western blotting analysis reveals high-molecular-weight soluble $A\beta_{42}$ species and insoluble aggregates, although to a lesser extent in the presence of L1 (Figure 8, lanes 4 and 7). In the presence of Cu^{2+}, either L1 or L2 partially inhibits the Cu^{2+}-promoted formation of small soluble aggregates and allows for enhanced $A\beta_{42}$ aggregation (Figure 8, panels 5 and 8 vs panel 2). This is supported by native gel/Western blotting, which shows that while there is a slightly increased amount of low-molecular-weight (10−80 kDa) soluble $A\beta_{42}$ species, more insoluble aggregates are also observed at the top of the gel (Figure 8, lanes 5 and 8). In the presence of Zn^{2+}, either L1 or L2 seems to have a limited effect on the morphology of the insoluble $A\beta_{42}$ aggregates, as observed by both TEM and Western blotting (Figure 8, panels/lanes 6 and 9). Overall, all of these in vitro studies suggest that compounds L1 and L2 should control the formation of Cu^{2+}-stabilized soluble $A\beta_{42}$ species and thus should control their neurotoxicity (vide infra).

Effect of L1 and L2 on the $A\beta_{42}$ Neurotoxicity. Because Cu^{2+}−$A\beta$ species have been shown to be neurotoxic,[20,21,31,51,52] the development of metal-binding compounds that control the metal-dependent $A\beta$ toxicity is desired. In this regard, the effect of L1 and L2 on the $A\beta_{42}$ neurotoxicity in N2A cells was investigated using an Alamar Blue cell viability assay.[53] First, we examined the toxicity of both L1 and L2 along with ethylenediaminetetraacetic acid (EDTA) and CQ at various concentrations ranging from 0.2 to 20 μM (Figure S11 in the SI).[40] Both L1 and L2 show no appreciable cell toxicity (>80%

dx.doi.org/10.1021/ic500926c | Inorg. Chem. 2014, 53, 11367−11376

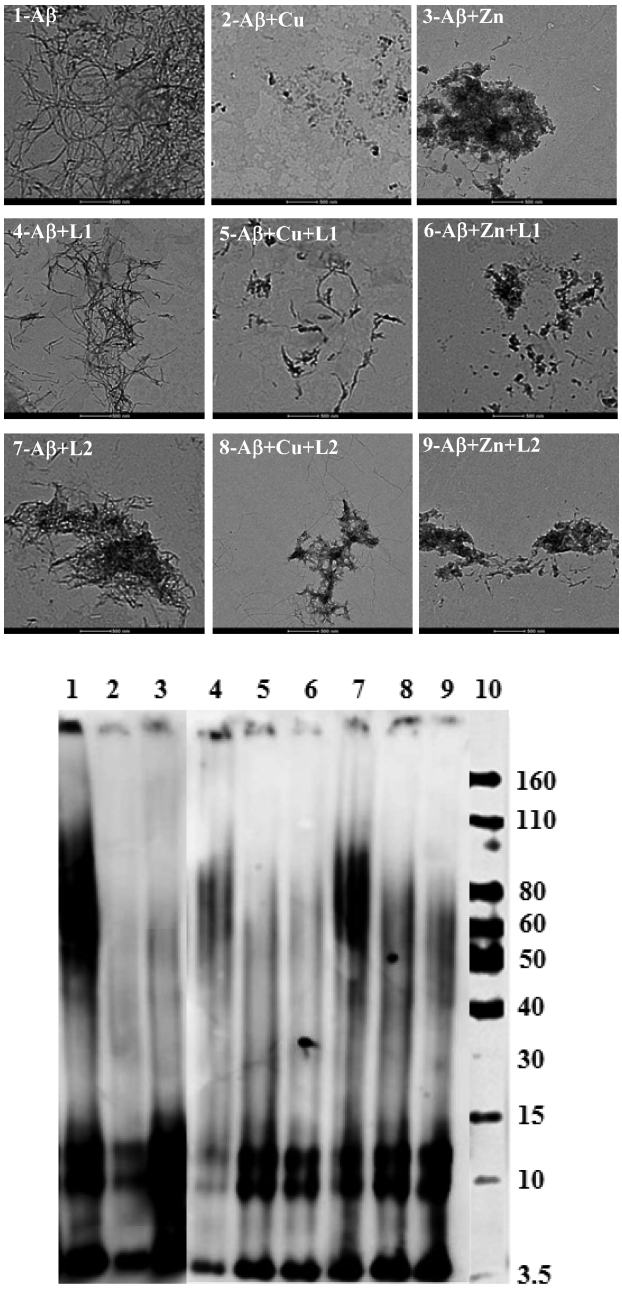

Figure 8. Top: TEM images of the disaggregation of $A\beta_{42}$ aggregation by L1 and L2, in the presence or absence of metal ions ($[A\beta_{42}] = [M^{2+}] = 25\ \mu M$; [compound] = 50 μM; PBS, 37 °C, 24 h for fibrilization and an additional 24 h for disaggregation, scale bar = 500 nm). Bottom: Native gel electrophoresis/Western blotting analysis. Panels and lanes are as follows: (1) $A\beta_{42}$; (2) $A\beta_{42} + Cu^{2+}$; (3) $A\beta_{42} + Zn^{2+}$; (4) $A\beta_{42}$ + L1; (5) $A\beta_{42}$ + L1 + Cu^{2+}; (6) $A\beta_{42}$ + L1 + Zn^{2+}; (7) $A\beta_{42}$ + L2; (8) $A\beta_{42}$ + L2 + Cu^{2+}; (9) $A\beta_{42}$ + L2 + Zn^{2+}; (10) MW marker.

cell survival) even up to 20 μM concentration. By comparison, the clinically tested compound CQ was quite toxic to cells even at 2 μM concentration, while EDTA does not show any toxicity up to 20 μM.[25,31] For the preformed $A\beta_{42}$ fibrils, no significant cell toxicity was observed in either the absence or presence of Cu^{2+} (Figure 9, lanes 1 and 2), supporting the previously reported diminished toxicity of $A\beta_{42}$ fibrils.[5,7,54−56] Moreover, compounds L1 and L2 do not affect the cell viability when added to the N2A cells in the presence of preformed $A\beta_{42}$ fibrils

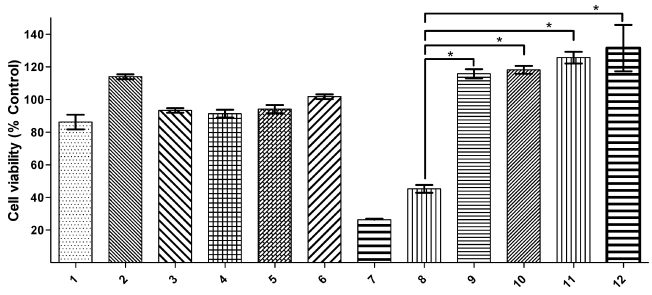

Figure 9. Cell viability (% DMSO control) of N2A cells determined by the Alamar Blue assay, upon incubation with (1) $A\beta_{42}$ fibrils, (2) $A\beta_{42}$ fibrils + Cu^{2+}, (3) $A\beta_{42}$ fibrils + L1, (4) $A\beta_{42}$ fibrils + L2, (5) $A\beta_{42}$ fibrils + Cu^{2+} + L1, (6) $A\beta_{42}$ fibrils + Cu^{2+} + L2, (7) $A\beta_{42}$ fibrils + Cu^{2+} + CQ, (8) $A\beta_{42}$ oligomers, (9) $A\beta_{42}$ oligomers + L1, (10) $A\beta_{42}$ oligomers + L2, (11) $A\beta_{42}$ oligomers + L1 + Cu^{2+}, and (12) $A\beta_{42}$ oligomers + L2 + Cu^{2+}. Conditions: [compound] = 20 μM; $[Cu^{2+}]$ = 20 μM; $[A\beta_{42}]$ = 20 μM. The *t*-test analysis reveals values of $p < 0.001$ for the pairs of data sets marked with asterisks.

(Figure 9, lanes 3 and 4). Even in the presence of preformed $A\beta_{42}$ fibrils and Cu^{2+}, the cell viability is not affected by either L1 or L2 (Figure 9, lanes 5 and 6). By contrast, CQ shows quite high cell toxicity to cells in the presence of Cu^{2+} and $A\beta_{42}$ fibrils with a cell survival of only 26 ± 3% (Figure 9, lane 7). Thus, these cellular toxicity data suggest that L1 and L2 do not lead to any cell toxicity in the presence or absence of $A\beta_{42}$ fibrils and Cu^{2+} ions, suggesting that these compounds do not disaggregate $A\beta_{42}$ fibrils to generate neurotoxic soluble $A\beta_{42}$ species.

As shown previously,[20,21] the preformed soluble $A\beta_{42}$ oligomers show a limited cell survival of 45 ± 6% (Figure 9, lane 8). Also, we have shown previously that while Cu^{2+} by itself is not toxic to N2A cells, the presence of Cu^{2+} and either monomeric $A\beta_{42}$ or soluble $A\beta_{42}$ oligomers exhibits enhanced cell toxicity.[17,18] However, the addition of either L1 or L2 to the N2A cells along with the preformed $A\beta_{42}$ oligomers drastically reduces the neurotoxicity of soluble $A\beta_{42}$ species to 100 ± 15% and 103 ± 15% cell viability, respectively (Figure 9, lanes 9 and 10). Even in the presence of Cu^{2+}, which has been shown to stabilize the soluble $A\beta_{42}$ oligomers,[22] L1 and L2 were able to eliminate the neurotoxicity of soluble $A\beta_{42}$ oligomers (Figure 9, lanes 9 and 10). These results are particularly exciting because, to the best of our knowledge, these are the first BFCs that reduce the toxicity of soluble $A\beta_{42}$ oligomers, in both the presence or absence of Cu^{2+} ions. These BFCs thus represent promising lead compounds for the development of potential therapeutic agents that can control the metal-mediated neurotoxicity of soluble $A\beta_{42}$ species in AD and are currently the focus of our ongoing in vivo studies.

■ CONCLUSION

In summary, two small BFCs, L1 and L2, were developed to specifically target the interactions of Cu^{2+} and Zn^{2+} ions with the $A\beta_{42}$ peptide and to control the formation of neurotoxic soluble $A\beta_{42}$ oligomers. The bifunctionality of L1 and L2 (i.e., metal chelation and $A\beta$ interaction) was established through various spectroscopic studies such as spectrophotometric titrations, structural characterization, and fluorescent assays. We have previously shown that BFCs, which have high affinity for both metal ions and $A\beta$ fibrils, can cause significant oligomerization via disaggregation of $A\beta_{42}$ fibrils and lead to enhanced neurotoxicity.[20] However, the BFCs described herein

dx.doi.org/10.1021/ic500926c | Inorg. Chem. 2014, 53, 11367−11376

bind to metal ions and Aβ fibrils only with moderate affinity and are having the desired opposite effect of promoting fibrillization of Cu^{2+}-stabilized soluble Aβ_{42} oligomers, and most importantly they drastically reduce the neurotoxicity of soluble Aβ_{42} species, in both the presence or absence Cu^{2+} ions. Because, to the best of our knowledge, these BFCs are the first to control the metal-mediated neurotoxicity of Aβ_{42} oligomers, L1 and L2 are promising lead compounds for the development of chemical agents that can control the neurotoxicity of soluble Aβ_{42} species in AD.

■ ASSOCIATED CONTENT

Supporting Information

X-ray crystallographic data in CIF format, synthetic schemes for L1 and L2, UV−vis and fluororescence spectra of L1 and L2, Job's plots for L1 in the presence of metal ions, UV−vis spectra of metal complexes, toxicity data of compounds, and X-ray data for **1**−**3**. This material is available free of charge via the Internet at http://pubs.acs.org.

■ AUTHOR INFORMATION

Corresponding Author

*E-mail: mirica@wustl.edu.

Notes

The authors declare no competing financial interest.

■ ACKNOWLEDGMENTS

We thank the Oak Ridge Associated Universities for a Ralph E. Powe Junior Faculty Award (to L.M.M.), the Washington University Knight Alzheimer's Disease Research Center (Pilot Research NIH Grant P50-AG05681 to L.M.M.), the Alzheimer's Association for New Investigator Research Grant NIRP-12-259199 (to L.M.M.), and the NIH Grant P30NS69329 (to J.K.) for financial support. L.M.M. is a Sloan Fellow.

■ REFERENCES

(1) Alzheimer's Disease Facts and Figures: Annual Report, 2013, from www.alz.org.
(2) Ferri, C. P.; Prince, M.; Brayne, C.; Brodaty, H.; Fratiglioni, L.; Ganguli, M.; Hall, K.; Hasegawa, K.; Hendrie, H.; Huang, Y.; Jorm, A.; Mathers, C.; Menezes, P. R.; Rimmer, E.; Scazufca, M. *Lancet* **2005**, *366*, 2112−2117.
(3) Jakob-Roetne, R.; Jacobsen, H. *Angew. Chem., Int. Ed.* **2009**, *48*, 3030−3059.
(4) Hardy, J.; Selkoe, D. J. *Science* **2002**, *297*, 353−356.
(5) Walsh, D. M.; Selkoe, D. J. *J. Neurochem.* **2007**, *101*, 1172−1184.
(6) Haass, C.; Selkoe, D. J. *Nat. Rev. Mol. Cell Biol.* **2007**, *8*, 101−112.
(7) Lambert, M. P.; Barlow, A. K.; Chromy, B. A.; Edwards, C.; Freed, R.; Liosatos, M.; Morgan, T. E.; Rozovsky, I.; Trommer, B.; Viola, K. L.; Wals, P.; Zhang, C.; Finch, C. E.; Krafft, G. A.; Klein, W. L. *Proc. Natl. Acad. Sci. U.S.A.* **1998**, *95*, 6448−6453.
(8) Gong, Y. S.; Chang, L.; Viola, K. L.; Lacor, P. N.; Lambert, M. P.; Finch, C. E.; Krafft, G. A.; Klein, W. L. *Proc. Natl. Acad. Sci. U.S.A.* **2003**, *100*, 10417−10422.
(9) McGowan, E.; Pickford, F.; Kim, J.; Onstead, L.; Eriksen, J.; Yu, C.; Skipper, L.; Murphy, M. P.; Beard, J.; Das, P.; Jansen, K.; DeLucia, M.; Lin, W. L.; Dolios, G.; Wang, R.; Eckman, C. B.; Dickson, D. W.; Hutton, M.; Hardy, J.; Golde, T. *Neuron* **2005**, *47*, 191−199.
(10) Kuperstein, I.; Broersen, K.; Benilova, I.; Rozenski, J.; Jonckheere, W.; Debulpaep, M.; Vandersteen, A.; Segers-Nolten, I.; Van Der Werf, K.; Subramaniam, V.; Braeken, D.; Callewaert, G.; Bartic, C.; D'Hooge, R.; Martins, I. C.; Rousseau, F.; Schymkowitz, J.; De Strooper, B. *EMBO J.* **2010**, *29*, 3408−3420.
(11) Lovell, M. A.; Robertson, J. D.; Teesdale, W. J.; Campbell, J. L.; Markesbery, W. R. *J. Neurol. Sci.* **1998**, *158*, 47−52.
(12) Bush, A. I.; Pettingell, W. H.; Multhaup, G.; Paradis, M. D.; Vonsattel, J. P.; Gusella, J. F.; Beyreuther, K.; Masters, C. L.; Tanzi, R. E. *Science* **1994**, *265*, 1464−1467.
(13) Atwood, C. S.; Moir, R. D.; Huang, X. D.; Scarpa, R. C.; Bacarra, N. M. E.; Romano, D. M.; Hartshorn, M. K.; Tanzi, R. E.; Bush, A. I. *J. Biol. Chem.* **1998**, *273*, 12817−12826.
(14) Hureau, C.; Faller, P. *Biochimie* **2009**, *91*, 1212.
(15) Zhu, X.; Su, B.; Wang, X.; Smith, M.; Perry, G. *Cell. Mol. Life Sci.* **2007**, *64*, 2202−2210.
(16) Crichton, R. R.; Dexter, D. T.; Ward, R. J. *Coord. Chem. Rev.* **2008**, *252*, 1189−1199.
(17) House, E.; Collingwood, J.; Khan, A.; Korchazkina, O.; Berthon, G.; Exley, C. *J. Alzheimer's Dis.* **2004**, *6*, 291−301.
(18) Exley, C. *J. Alzheimer's Dis.* **2006**, *10*, 173−177.
(19) Exley, C. *Coord. Chem. Rev.* **2012**, *256*, 3114−3114.
(20) Sharma, A. K.; Pavlova, S. T.; Kim, J.; Finkelstein, D.; Hawco, N. J.; Rath, N. P.; Kim, J.; Mirica, L. M. *J. Am. Chem. Soc.* **2012**, *134*, 6625−6636.
(21) Sharma, A. K.; Pavlova, S. T.; Kim, J.; Kim, J.; Mirica, L. M. *Metallomics* **2013**, *5*, 1529−1536.
(22) Zhang, Y.; Rempel, D. L.; Zhang, J.; Sharma, A. K.; Mirica, L. M.; Gross, M. L. *Proc. Natl. Acad. Sci. U.S.A.* **2013**, *110*, 14604−14609.
(23) Rodríguez-Rodríguez, C.; Telpoukhovskaia, M.; Orvig, C. *Coord. Chem. Rev.* **2012**, *256*, 2308−2332.
(24) Braymer, J. J.; DeToma, A. S.; Choi, J.-S.; Ko, K. S.; Lim, M. H. *Int. J. Alzheimer's Dis.* **2011**, *2011*, ID 623051.
(25) Choi, J.-S.; Braymer, J. J.; Nanga, R. P. R.; Ramamoorthy, A.; Lim, M. H. *Proc. Natl. Acad. Sci. U.S.A.* **2010**, *107*, 21990−21995.
(26) Scott, L. E.; Orvig, C. *Chem. Rev.* **2009**, *109*, 4885−4910.
(27) Dedeoglu, A.; Cormier, K.; Payton, S.; Tseitlin, K. A.; Kremsky, J. N.; Lai, L.; Li, X. H.; Moir, R. D.; Tanzi, R. E.; Bush, A. I.; Kowall, N. W.; Rogers, J. T.; Huang, X. D. *Exp. Gerontol.* **2004**, *39*, 1641−1649.
(28) Liu, Y. Z.; Kochi, A.; Pithadia, A. S.; Lee, S.; Nam, Y.; Beck, M. W.; He, X. M.; Lee, D.; Lim, M. H. *Inorg. Chem.* **2013**, *52*, 8121−8130.
(29) Pithadia, A. S.; Lim, M. H. *Curr. Opin. Chem. Biol.* **2012**, *16*, 67−73.
(30) Pithadia, A. S.; Kochi, A.; Soper, M. T.; Beck, M. W.; Liu, Y. Z.; Lee, S.; DeToma, A. S.; Ruotolo, B. T.; Lim, M. H. *Inorg. Chem.* **2012**, *51*, 12959−12967.
(31) Hindo, S. S.; Mancino, A. M.; Braymer, J. J.; Liu, Y. H.; Vivekanandan, S.; Ramamoorthy, A.; Lim, M. H. *J. Am. Chem. Soc.* **2009**, *131*, 16663.
(32) Scott, L. E.; Telpoukhovskaia, M.; Rodriguez-Rodriguez, C.; Merkel, M.; Bowen, M. L.; Page, B. D. G.; Green, D. E.; Storr, T.; Thomas, F.; Allen, D. D.; Lockman, P. R.; Patrick, B. O.; Adam, M. J.; Orvig, C. *Chem. Sci.* **2011**, *2*, 642.
(33) Rodriguez-Rodriguez, C.; de Groot, N. S.; Rimola, A.; Alvarez-Larena, A.; Lloveras, V.; Vidal-Gancedo, J.; Ventura, S.; Vendrell, J.; Sodupe, M.; Gonzalez-Duarte, P. *J. Am. Chem. Soc.* **2009**, *131*, 1436−1451.
(34) Braymer, J. J.; DeToma, A. S.; Choi, J.-S.; Ko, K. S.; Lim, M. H. *Int. J. Alzheimer's Dis.* **2011**, *2011*, 623051.
(35) Bruker Analytical X-ray: Madison, WI, 2008.
(36) Sheldrick, G. M. *Acta Crystallogr.* **2008**, *A64*, 112−122.
(37) Gans, P.; Sabatini, A.; Vacca, A. *Ann. Chim.* **1999**, 45.
(38) Alderighi, L. *Coord. Chem. Rev.* **1999**, *184*, 311.
(39) Klein, W. L. *Neurochem. Int.* **2002**, *41*, 345−352.
(40) See the SI.
(41) Lipinski, C. A.; Lombardo, F.; Dominy, B. W.; Feeney, P. J. *Adv. Drug Delivery Rev.* **2001**, *46*, 3−26.
(42) Storr, T.; Merkel, M.; Song-Zhao, G. X.; Scott, L. E.; Green, D. E.; Bowen, M. L.; Thompson, K. H.; Patrick, B. O.; Schugar, H. J.; Orvig, C. *J. Am. Chem. Soc.* **2007**, *129*, 7453−7463.
(43) Huang, C. Y. *Methods Enzymol.* **1982**, *87*, 509.
(44) Talmard, C.; Bouzan, A.; Faller, P. *Biochemistry* **2007**, *46*, 13658−13666.

(45) Klunk, W. E.; Wang, Y. M.; Huang, G. F.; Debnath, M. L.; Holt, D. P.; Mathis, C. A. *Life Sci.* **2001**, *69*, 1471−1484.
(46) LeVine, H., 3rd. *Methods Enzymol.* **1999**, *309*, 274−284.
(47) Lockhart, A.; Ye, L.; Judd, D. B.; Merritt, A. T.; Lowe, P. N.; Morgenstern, J. L.; Hong, G. Z.; Gee, A. D.; Brown, J. *J. Biol. Chem.* **2005**, *280*, 7677−7684.
(48) Haass, C.; Selkoe, D. J. *Nat. Rev. Mol. Cell Biol.* **2007**, *8*, 101−112.
(49) Mold, M.; Ouro-Gnao, L.; Wieckowski, B. M.; Exley, C. *Sci. Rep.* **2013**, *3*.
(50) House, E.; Mold, M.; Collingwood, J.; Baldwin, A.; Goodwin, S.; Exley, C. *J. Alzheimer's Dis.* **2009**, *18*, 811−817.
(51) Bush, A. I. *Neurobiol. Aging* **2002**, *23*, 1031−1038.
(52) Huang, X. D.; Cuajungco, M. P.; Atwood, C. S.; Hartshorn, M. A.; Tyndall, J. D. A.; Hanson, G. R.; Stokes, K. C.; Leopold, M.; Multhaup, G.; Goldstein, L. E.; Scarpa, R. C.; Saunders, A. J.; Lim, J.; Moir, R. D.; Glabe, C.; Bowden, E. F.; Masters, C. L.; Fairlie, D. P.; Tanzi, R. E.; Bush, A. I. *J. Biol. Chem.* **1999**, *274*, 37111−37116.
(53) Dahlgren, K. N.; Manelli, A. M.; Stine, W. B.; Baker, L. K.; Krafft, G. A.; LaDu, M. J. *J. Biol. Chem.* **2002**, *277*, 32046−32053.
(54) Hsia, A. Y.; Masliah, E.; McConlogue, L.; Yu, G.-Q.; Tatsuno, G.; Hu, K.; Kholodenko, D.; Malenka, R. C.; Nicoll, R. A.; Mucke, L. *Proc. Natl. Acad. Sci. U.S.A.* **1999**, *96*, 3228−3233.
(55) Lesne, S.; Koh, M. T.; Kotilinek, L.; Kayed, R.; Glabe, C. G.; Yang, A.; Gallagher, M.; Ashe, K. H. *Nature* **2006**, *440*, 352−357.
(56) Ahmed, M.; Davis, J.; Aucoin, D.; Sato, T.; Ahuja, S.; Aimoto, S.; Elliott, J. I.; Van Nostrand, W. E.; Smith, S. O. *Nat. Struct. Mol. Biol.* **2011**, *17*, 561−567.